Mineralogical Magazine (2019), **83**, 799–808
doi:10.1180/mgm.2019.34

CAMBRIDGE
UNIVERSITY PRESS

Article

Lussierite, a new sodium uranyl sulfate mineral with bidentate $UO_7–SO_4$ linkage from the Blue Lizard mine, San Juan County, Utah, USA

Anthony R. Kampf[1*], Travis A. Olds[2†], Jakub Plášil[3], Barbara P. Nash[4] and Joe Marty[5]

[1]Mineral Sciences Department, Natural History Museum of Los Angeles County, 900 Exposition Boulevard, Los Angeles, CA 90007, USA; [2]Department of Civil and Environmental Engineering and Earth Sciences, University of Notre Dame, Notre Dame, IN 46556, USA; [3]Institute of Physics ASCR, v.v.i., Na Slovance 1999/2, 18221 Prague 8, Czech Republic; [4]Department of Geology and Geophysics, University of Utah, Salt Lake City, UT 84112, USA; and [5]5199 East Silver Oak Road, Salt Lake City, UT 84108, USA

Abstract

The new mineral lussierite (IMA2018-101), $Na_{10}[(UO_2)(SO_4)_4](SO_4)_2(H_2O)_3$, was found in the Blue Lizard mine, San Juan County, Utah, USA, where it occurs as pale green–yellow prisms or blades in a secondary assemblage with belakovskiite, ferrinatrite, halite, ivsite, metavoltine and thénardite. The streak is white and the fluorescence is bright cyan under 365 nm ultraviolet light. Crystals are transparent with vitreous lustre. The tenacity is brittle, the Mohs hardness is 2½, the fracture is irregular and no cleavage was observed. The mineral is easily soluble in H_2O and has a measured density of 2.87(2) g cm^{-3}. Lussierite is optically biaxial (+), with $\alpha = 1.493(1)$, $\beta = 1.505(1)$ and $\gamma = 1.518(1)$ (white light); $2V_{meas.} = 88(1)°$; dispersion is $r > v$, moderate; pleochroism: X = colourless, Y and Z = green yellow ($X < Y \approx Z$); optical orientation: $X = \mathbf{b}$, $Z \wedge \mathbf{a} = 44°$ in obtuse β. Electron microprobe analyses (wavelength-dispersive spectroscopy mode) provided $Na_{10}(U_{0.99}O_2)(S_{1.00}O_4)_6{\cdot}3H_2O$ (+0.06 H for charge balance). The five strongest X-ray powder diffraction lines are [d_{obs} Å(I)(hkl)]: 6.69(95)($\bar{1}11$,130), 4.814(100)(150,002,060), 3.461(83)(171,$\bar{2}02$), 2.955(81)(113,330) and 2.882(74)($\bar{1}91$,311,191,0·10·0). Lussierite is monoclinic, Cc, $a = 9.3134(4)$, $b = 28.7501(11)$, $c = 9.6346(7)$ Å, $\beta = 93.442(7)°$, $V = 2575.1(2)$ Å^3 and $Z = 4$. The structure ($R_1 = 0.0298$ for 5202 $I > 2\sigma I$) contains a $[(UO_2)(SO_4)_4]^{6-}$ uranyl sulfate cluster in which one SO_4 tetrahedron shares an edge (bidentate linkage) with the UO_7 pentagonal bipyramid. The uranyl sulfate clusters occur in layers and are linked through a complex network of bonds involving Na^+ cations, isolated SO_4 tetrahedra and isolated H_2O groups.

Keywords: lussierite, new mineral, uranyl sulfate, crystal structure, Blue Lizard mine, Red Canyon, Utah, USA

(Received 22 March 2019; accepted 23 April 2019; Accepted Manuscript published online: 3 June 2019; Associate Editor: Daniel Atencio)

Introduction

The Blue Lizard mine in Red Canyon, Utah, USA, has proven to be a remarkable source of new minerals, especially sodium uranyl sulfates. Lussierite, $Na_{10}[(UO_2)(SO_4)_4](SO_4)_2(H_2O)_3$, is the 13th new sodium uranyl sulfate mineral to be described from the mine and several more potentially new sodium uranyl sulfate minerals are currently under study. The astounding diversity and relatively high structural complexity of sodium uranyl sulfate minerals has been highlighted recently by Gurzhiy and Plášil (2019). A large number of stable combinatorial linkages of uranyl and sulfate tetrahedra are possible, with the topological arrangements appearing to be strongly affected by at least three parameters: pH (Plášil *et al.*, 2014); cation content; and water content. In general, sodium uranyl sulfate minerals follow the same structure topology trends as do other uranyl minerals (Lussier *et al.*, 2016), where uranyl polyhedra preferentially polymerise into extended structures *via* linkages of their equatorial vertices, most often forming infinite chain or infinite sheet topologies. However, cluster topologies, such as that found in lussierite, are relatively abundant among the sodium uranyl sulfate minerals, for reasons that are not completely clear. Understanding the hierarchical arrangements of these structures and how conditions of formation influence the crystallised topologies is important to understanding the crystal–chemical nature of U–S systems, and for uranyl mineralogy as a whole.

Lussierite (/lu: ’si: ei ait/) is named in honour of Canadian mineralogist Aaron J. Lussier (born 1980). Dr. Lussier received his Ph.D. in mineralogy and crystallography from the University of Manitoba in 2012, studying zonation in tourmaline from granitic pegmatites and the occurrence of tetrahedrally co-ordinated aluminium and boron in tourmaline (Lussier, 2012). Dr. Lussier held a Post-Doctoral Research Fellowship at the University of Notre Dame from 2012 to 2015, investigating the crystal–chemistry of actinide elements with support from the Natural Sciences and Engineering Research Council (NSERC). He is currently a Research Scientist at the Canadian Museum of Nature and Councilor of the Mineralogical Association of Canada since 2017. Dr. Lussier has been involved in the descriptions of four new minerals, fluor-elbaite (Bosi *et al.*,

---

*Author for correspondence: Anthony R. Kampf, Email: akampf@nhm.org

[†]Current address: Section of Minerals, Carnegie Museum of Natural History, 4400 Forbes Avenue, Pittsburgh, PA 15213, USA

Cite this article: Kampf A.R., Olds T.A., Plášil J., Nash B.P. and Marty J. (2019) Lussierite, a new sodium uranyl sulfate mineral with bidentate $UO_7–SO_4$ linkage from the Blue Lizard mine, San Juan County, Utah, USA. *Mineralogical Magazine* **83**, 799–808. https://doi.org/10.1180/mgm.2019.34

2013), ferro-ferri-nybøite (Lussier *et al.*, 2014), maruyamaite (Hawthorne *et al.*, 2016) and shinkolobweite (Olds *et al.*, 2017). He has authored or co-authored several articles that advance our understanding of actinide mineralogy and crystal chemistry, and was senior author of a comprehensive review of the structures of uranyl compounds: "*A revised and expanded structure hierarchy of natural and synthetic hexavalent uranium compounds*" (Lussier *et al.*, 2016). Dr. Lussier has given permission for this mineral to be named in his honour.

The new mineral and name were approved by the Commission on New Minerals, Nomenclature and Classification of the International Mineralogical Association (IMA2018-101, Kampf *et al.*, 2018). The description is based on one holotype and two cotype specimens deposited in the collections of the Natural History Museum of Los Angeles County, 900 Exposition Boulevard, Los Angeles, CA 90007, USA, catalogue numbers 73518 (holotype), 73519 (cotype) and 73520 (cotype).

Occurrence

Lussierite was found underground in the Blue Lizard mine (37°33′26″N, 110°17′44″W), Red Canyon, White Canyon District, San Juan County, Utah, USA. The mine is ~72 km west of the town of Blanding, Utah, and ~22 km southeast of Good Hope Bay on Lake Powell. The following information on the mine and its geology is taken largely from Chenoweth (1993).

The uranium deposits in Red Canyon occur within the Shinarump member of the Upper Triassic Chinle Formation, in channels incised into the reddish-brown siltstones of the underlying Lower Triassic Moenkopi Formation. The Shinarump member consists of medium- to coarse-grained sandstone, conglomeratic sandstone beds and thick siltstone lenses. Ore minerals were deposited as replacements of wood and other organic material and as disseminations in the enclosing sandstone. Since the mine closed in 1978, oxidation of primary ores in the humid underground environment has produced a variety of secondary minerals, mainly sulfates, as efflorescent crusts on the surfaces of mine walls.

Lussierite is a rare mineral in the secondary mineral assemblages of the Blue Lizard mine. It occurs on a thick crust of gypsum overlaying matrix comprised mostly of subhedral to euhedral, equant quartz crystals that are recrystallised counterparts of the original grains of the sandstone. Other secondary phases found in close association with lussierite are belakovskiite, ferrinatrite, halite, ivsite, metavoltine, thénardite and at least three other potentially new minerals. Lussierite is the 19th new mineral to be described from the Blue Lizard mine, all within the last 6 years (*cf.* Kampf *et al.*, 2017), and numerous more new phases await characterisation.

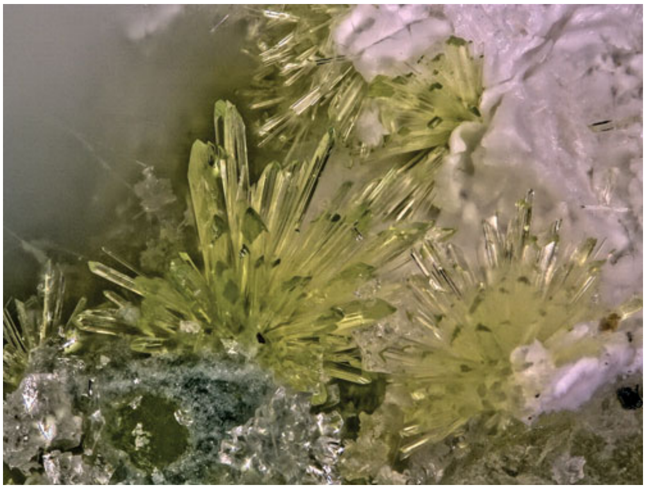

Fig. 1. Sprays of greenish yellow lussierite prisms with opaque white thénardite. The field of view is 1.7 mm across.

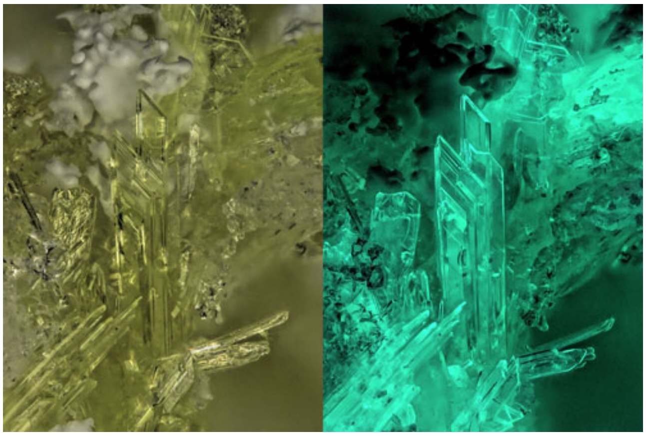

Fig. 2. Lussierite blades in incandescent (left) and 365 nm ultraviolet (right) illumination. The field of view is 0.84 mm across.

Physical and optical properties

Lussierite crystals are prisms or blades, elongate on [001] and sometimes flattened on {010}, up to ~0.5 mm long. Prisms tend to occur in sprays (Fig. 1) or randomly scattered individuals; blades tend to occur in parallel growths (Fig. 2). Crystals exhibit the prism forms {010}, {110} and $\{\bar{1}\bar{1}0\}$, and have angled, wedge-like terminations composed of a series of $\{\bar{1}k1\}$ forms: $\{\bar{1}11\}$,

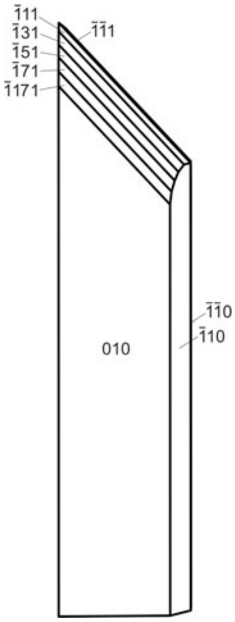

Fig. 3. Crystal drawing of lussierite; clinographic projection in non-standard orientation.

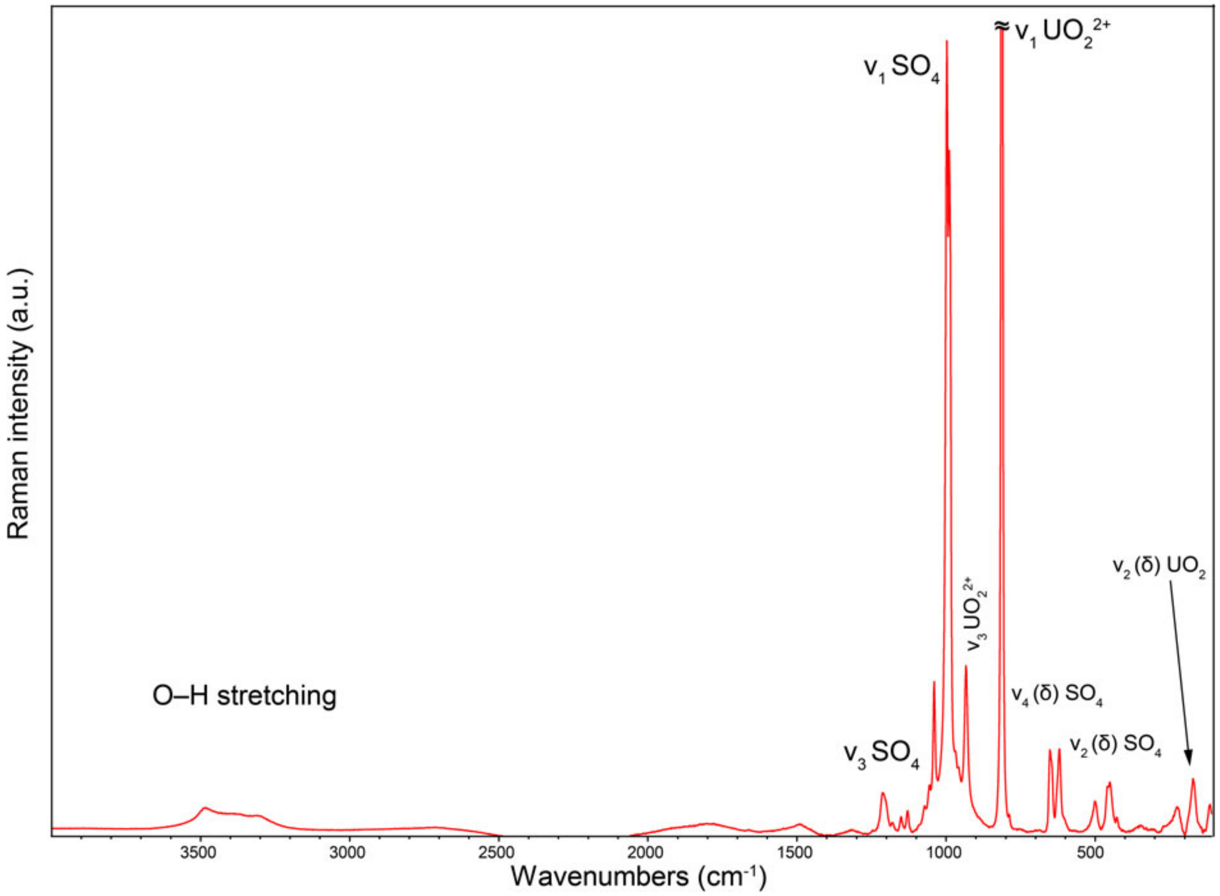

Fig. 4. The baseline-corrected Raman spectrum of lussierite recorded with a 532 nm laser.

$\{\bar{1}31\}$, $\{\bar{1}51\}$, $\{\bar{1}71\}$ and $\{\bar{1}{\cdot}17{\cdot}1\}$ (Fig. 3). Twinning was not observed visually, but the structure refinement indicates twinning by merohedry, as is typical of noncentrosymmetric crystals.

The mineral is light greenish yellow with a white streak and fluoresces bright cyan under 365 nm ultraviolet illumination (Fig. 2). Crystals are transparent and have a vitreous lustre. The tenacity is brittle, the Mohs hardness is 2½ (based on scratch tests), the fracture is irregular and no cleavage was observed. The density measured by flotation in methylene iodide–toluene is 2.87(2) g cm^{-3}. The calculated density is 2.907 g cm^{-3} for the empirical formula and 2.912 g cm^{-3} for the ideal formula. At room temperature, the mineral is easily soluble in H_2O.

Optically, lussierite is biaxial (+), with $\alpha = 1.493(1)$, $\beta = 1.505(1)$ and $\gamma = 1.518(1)$ (measured in white light). The 2V measured directly on a spindle stage is 88(1)°; the calculated 2V is 88.4°. Dispersion is $r > v$, moderate. The mineral is pleochroic: X = colourless, Y and Z = green yellow; $X < Y \approx Z$. The optical orientation is $X = \mathbf{b}$, $Z \wedge \mathbf{a} = 44°$ in obtuse β. The Gladstone–Dale compatibility, $1 - (K_P/K_C)$, is –0.001 (superior) based on the empirical formula using $k(UO_3) = 0.118$, as provided by Mandarino (1976).

Table 1. Chemical composition of lussierite.

Constituent	Mean	Range	S.D.	Standard
Na_2O	(24.83)	23.98–25.84	0.68	Albite
Na_2O*	28.31			
UO_3	25.79	25.41–26.04	0.24	Synthetic UO_2
SO_3	43.89	43.17–44.41	0.46	Celestine
H_2O*	5.00			
Total	102.99			

S.D. – standard deviation; * based on the structure.

Raman spectroscopy

Raman spectroscopy was conducted on a Horiba XploRA PLUS both with 532 nm and 785 nm diode lasers. Some fluorescence was observed with the 532 nm laser, but it was relatively minor, so this spectrum is reported. The spectrum was recorded from 4000 to 100 cm^{-1} (Fig. 4) using a 50 μm laser slit, 1800 gr/mm diffraction grating, 100× (0.9 N.A.) objective and 15.2 mW laser power at the sample, with a beam diameter of ~1.2 μm.

A broad band of weak intensity in the range ~3600–3200 cm^{-1} is attributed to the stretching vibrations of H_2O molecules. According to the correlation given by Libowitzky (1999), the approximate O–H···O hydrogen bond lengths range between 3.2 and 2.8 Å. There are a few broad weak bands located between ~1700–1450 cm^{-1}, in the region expected for the ν_2 (δ) bending vibrations of H_2O molecules; however, we conclude that the observed features are more likely to be due to fluorescence because they were not observed in the spectrum recorded using the 785 nm diode laser.

Several past studies of uranyl sulfates informed our assignments of bands to specific Raman modes (*cf.* Plášil *et al.*, 2010; Čejka, 1999). In the lussierite spectrum, the split, triply degenerate

Table 2. Powder X-ray data (*d* in Å) for lussierite. Only calculated lines with *I* ≥ 3 are listed.

I_{obs}	d_{obs}	d_{calc}	I_{calc}	*h k l*
50	14.41	14.3751	70	0 2 0
39	8.87	8.8456	59	1 1 0
63	8.00	7.9933	78	0 2 1
17	7.20	7.1875	28	0 4 0
95	6.69	6.7041, 6.6728	57, 63	$\bar{1}$ 1 1, 1 3 0
15	6.31	6.3328	23	1 1 1
68	5.75	5.7573	69	0 4 1
		5.5965	9	$\bar{1}$ 3 1
100	4.814	4.8902, 4.8086, 4.7917	26, 8, 100	1 5 0, 0 0 2, 0 6 0
		4.6483	8	2 0 0
26	4.579	4.5602	32	0 2 2
49	4.419	4.4228, 4.4158	13, 52	2 2 0, $\bar{1}$ 5 1
29	4.323	4.3298, 4.3045	17, 22	$\bar{1}$ 1 2, 1 5 1
25	4.117	4.1270, 4.1083	9, 25	1 1 2, $\bar{2}$ 2 1
		3.9967	6	0 4 2
27	3.958	3.9835, 3.9339	20, 14	$\bar{1}$ 3 2, 2 2 1
		3.9032	10	2 4 0
18	3.829	3.8238	23	1 3 2
7	3.687	3.6819	17	$\bar{2}$ 4 1
46	3.569	3.5938, 3.5548	25, 38	0 8 0, 2 4 1
		3.5285	8	$\bar{1}$ 7 1
		3.4841	9	$\bar{1}$ 5 2
83	3.461	3.4709, 3.4471	29, 81	1 7 1, $\bar{2}$ 0 2
25	3.381	3.3942, 3.3758	11, 10	0 6 2, 1 5 2
		3.3664	7	0 8 1
		3.3521	7	$\bar{2}$ 2 2
		3.3364	3	2 6 0
32	3.154	3.1664	42	2 2 2
		3.1289	10	0 2 3
		3.1109	4	2 6 1
		3.1081	8	$\bar{2}$ 4 2
14	3.086	3.0810, 3.0706	9, 12	3 1 0, $\bar{1}$ 1 3
14	3.007	3.0211, 2.9864	12, 11	1 9 0, $\bar{3}$ 1 1
		2.9602, 2.9485	63, 10	1 1 3, 3 3 0
		2.9394	7	$\bar{1}$ 3 3
		2.9277	17	0 4 3
74	2.882	2.8984, 2.8845, 2.8750, 2.8663	16, 57, 13, 16	$\bar{1}$ 9 1, 3 1 1, 0 10 0, 1 9 1
		2.8431	10	2 8 0
58	2.799	2.7982	75	$\bar{2}$ 6 2
11	2.734	2.7546, 2.7279, 2.7207	13, 4, 9	0 10 1, 3 5 0, $\bar{1}$ 5 3
		2.6997	4	2 8 1
26	2.691	2.6875	25	2 6 2
		2.6691	7	$\bar{2}$ 2 3
21	2.654	2.6616, 2.6430	10, 24	$\bar{3}$ 5 1, 1 5 3
18	2.588	2.5887, 2.5802	16, 18	3 5 1, $\bar{3}$ 3 2
		2.5409	7	$\bar{2}$ 4 3
		2.5359	3	1 9 2
9	2.535	2.5279	10	2 2 3
		2.5161	3	1 11 0
		2.4683	6	$\bar{1}$ 7 3
11	2.441	2.4520, 2.4439	7, 5	3 3 2, $\bar{1}$ 11 1
		2.4284	4	$\bar{3}$ 5 2
		2.4245	6	1 11 1
28	2.398	2.4099, 2.3958	11, 13	1 7 3, 0 12 0
		2.3923	3	0 8 3
		2.3878	6	$\bar{2}$ 10 1
		2.3714	3	0 2 4
10	2.356	2.3685, 2.3544, 2.3520	6, 3, 9	3 7 1, $\bar{1}$ 1 4, 2 10 1
		2.3242	4	4 0 0
		2.3207	3	3 5 2
16	2.288	2.2937, 2.2908, 2.2801	8, 9, 8	$\bar{1}$ 3 4, $\bar{3}$ 1 3, 0 4 4
		2.2622	7	$\bar{4}$ 2 1
		2.2315	6	1 3 4
14	2.219	2.2243, 2.2146, 2.2114	4, 4, 5	3 9 0, 1 11 2, 4 4 0
		2.1899	5	$\bar{2}$ 0 4
12	2.174	2.1826, 2.1649, 2.1580	7, 3, 11	$\bar{4}$ 4 1, $\bar{2}$ 2 4, 3 1 3
		2.1522	3	2 10 2
29	2.141	2.1490, 2.1436, 2.1403, 2.1311, 2.1288	3, 8, 5, 3, 14	0 6 4, $\bar{4}$ 0 2, 0 10 3, 1 5 4, 4 4 1,
		2.1201	4	$\bar{4}$ 2 2
20	2.098	2.1059, 2.0948, 2.0934, 2.0911, 2.0851	10, 3, 8, 3, 7	$\bar{1}$ 13 1, $\bar{2}$ 4 4, 1 13 1, 4 6 0, 2 0 4

(*Continued*)

Table 2. (*Continued.*)

I_{obs}	d_{obs}	d_{calc}	I_{calc}	*h k l*
		2.0635	3	2 2 4
9	2.054	2.0536	11	0 14 0
		2.0450	3	4 0 2
6	2.014	2.0254	10	3 5 3
18	1.995	2.0055, 1.9983, 1.9951, 1.9917	4, 8, 7, 6	$\bar{3}$ 7 3, 0 8 4, $\bar{1}$ 11 3, $\bar{2}$ 6 4
		1.9744	4	$\bar{2}$ 10 3
		1.9714	4	$\bar{3}$ 11 1
		1.9638	3	1 11 3
18	1.956	1.9567, 1.9516, 1.9412	5, 14, 7	$\bar{4}$ 6 2, 4 8 0, 3 11 1
24	1.923	1.9277, 1.9204, 1.9178, 1.9146	12, 4, 3, 10	2 12 2, $\bar{4}$ 2 3, $\bar{3}$ 3 4, 3 7 3
		1.9119	4	2 6 4
26	1.902	1.9022	23	$\bar{1}$ 1 5
		1.8994	3	$\bar{1}$ 9 4
		1.8941	3	4 8 1
		1.8886	4	0 14 2
20	1.872	1.8809, 1.8772, 1.8710, 1.8700	7, 4, 5, 5	4 6 2, 1 15 0, $\bar{4}$ 4 3, $\bar{2}$ 8 4
		1.8655	3	$\bar{3}$ 9 3
23	1.845	1.8581, 1.8425, 1.8410	8, 18, 4	0 4 5, $\bar{5}$ 1 1, $\bar{4}$ 8 2
		1.8253	3	5 3 0
		1.8202	4	3 11 2
29	1.809	1.8155, 1.8133, 1.8095, 1.8035, 1.8019, 1.7981	4, 5, 9, 6, 6, 8	4 2 3, 3 3 4, $\bar{1}$ 5 5, 2 8 4, 5 1 1, $\bar{1}$ 13 3
16	1.784	1.7916, 1.7807, 1.7774, 1.7751	7, 7, 4, 5	$\bar{4}$ 10 1, $\bar{3}$ 13 1, 4 8 2, 1 13 3
		1.7736	3	4 4 3
35	1.762	1.7663, 1.7642, 1.7609, 1.7579, 1.7559	6, 8, 5, 21, 3	0 16 1, $\bar{2}$ 14 2, $\bar{2}$ 4 5, $\bar{5}$ 5 1, $\bar{1}$ 15 2
33	1.728	1.7415, 1.7355, 1.7292, 1.7281, 1.7258, 1.7243, 1.7236	6, 8, 6, 5, 3, 3, 20	1 15 2, 2 14 2, $\bar{1}$ 7 5, 2 2 5, $\bar{3}$ 11 3, 1 11 4, $\bar{4}$ 0 4
		1.7056	3	$\bar{4}$ 8 3
16	1.684	1.6971, 1.6918, 1.6840, 1.6741	5, 5, 6, 3	0 12 4, 2 4 5, $\bar{5}$ 7 1, 5 3 2
		1.6690	3	$\bar{3}$ 9 4
		1.6682	4	4 12 0
		1.6572	3	$\bar{2}$ 16 1
		1.6451	3	2 16 1
15	1.630	1.6366, 1.6309, 1.6301, 1.6285	3, 4, 3, 3	1 17 1, 4 8 3, 3 15 0, $\bar{1}$ 15 3
		1.6231	4	4 0 4
		1.6218	4	$\bar{4}$ 6 4
12	1.602	1.6069, 1.5988, 1.5975, 1.5935, 1.5895	3, 4, 5, 7, 3	$\bar{4}$ 10 3, 3 9 4, $\bar{4}$ 12 2, $\bar{3}$ 13 3, 3 1 5
13	1.574	1.5740, 1.5728	3, 6	$\bar{1}$ 3 6, 2 12 4
11	1.558	1.5674, 1.5666, 1.5657, 1.5554	5, 3, 3, 7	0 16 3, 2 8 5, 5 1 3, 4 12 2
13	1.537	1.5435, 1.5402, 1.5373, 1.5353	5, 4, 3, 7	1 3 6, $\bar{1}$ 11 5, 4 6 4, $\bar{2}$ 2 6
17	1.502	1.5105, 1.5082, 1.4987, 1.4969, 1.4932	4, 3, 3, 3, 4	2 18 0, 3 11 4, $\bar{2}$ 16 3, $\bar{5}$ 3 4, $\bar{6}$ 2 2
23	1.477	1.4880, 1.4844, 1.4829, 1.4780, 1.4737, 1.4722, 1.4704	6, 6, 4, 4, 5, 3, 3	2 0 6, 3 7 5, $\bar{4}$ 14 2, $\bar{1}$ 19 1, 1 19 1, 2 16 3, 1 17 3
		1.4649	3	5 7 3
		1.4631	3	2 14 4
10	1.449	1.4496, 1.4491, 1.4440	3, 3, 5	6 0 2, 4 14 2, $\bar{1}$ 13 5
		1.4301	3	$\bar{3}$ 17 2
16	1.421	1.4228, 1.4211, 1.4173, 1.4138	3, 5, 7, 3	6 8 0, 2 6 6, $\bar{5}$ 13 1, $\bar{4}$ 16 1

ν_3 $(SO_4)^{2-}$ antisymmetric stretching vibrations occur as weaker bands at 1210 (with a shoulder at 1195), 1180, 1150 and 1130 cm^{-1}. Weak bands at 1070 and 1040 cm^{-1} can be also related to ν_3 $(SO_4)^{2-}$; the increased number of observed bands related to antisymmetric stretching vibrations is due to the fact that there are six symmetrically non-equivalent SO_4 tetrahedra in the structure. The medium-strong bands at 998 and 989 cm^{-1} are unambiguously assignable to the ν_1 $(SO_4)^{2-}$ symmetric stretching vibrations. The weak band at 933 cm^{-1} is related with the ν_3 $(UO_2)^{2+}$ antisymmetric stretching vibrations. The ν_1 $(UO_2)^{2+}$ symmetric stretching vibration is present as a very strong band at 813 cm^{-1}. Bartlett and Cooney (1989) provided an empirical relationship to derive the approximate U–O_{Ur} bond lengths from the band positions assigned to the $(UO_2)^{2+}$ stretching vibrations, which gives 1.80 Å (ν_1) and 1.76 Å (ν_3), in accordance with U–O_{Ur} bond lengths from the X-ray data (1.77 Å and 1.78 Å).

Weak bands observed at 651 (with a shoulder at 645) and 620 cm^{-1} (with a shoulder at 627) are attributed to the split, triply degenerate ν_4 (δ) $(SO_4)^{2-}$ bending vibrations, and those at 500, 459, 450 and 427 cm^{-1} to the split doubly degenerate ν_2 (δ) $(SO_4)^{2-}$ bending vibrations. A weak band at 374 cm^{-1} is either due to ν (U–O_{eq}) stretching vibrations or Na–O stretches (e.g. Volkovich *et al.*, 1998; Plášil *et al.*, 2010; Kampf *et al.*, 2015). Bands at 267 and 225 cm^{-1} arise from ν_2 (δ) U–O–U bending modes. The bands at the lowest frequencies are attributable to further unassigned phonons.

Composition

Chemical analyses (6 points on 3 crystals) were performed using a Cameca SX-50 electron microprobe operating at an accelerating voltage of 15 kV, with a beam current of 10 nA and 20 μm spot diameter. Matrix effects were accounted for using the *PAP* correction routine (Pouchou and Pichoir, 1985). The sample exhibited substantial damage from the electron beam. The phase is very susceptible to Na migration under the electron beam. Efforts to correct for this with very short count times or translating the sample under the beam during analysis, as well as zero-time corrections

Table 3. Data collection and structure refinement details for lussierite.

Crystal data	
Structural formula	$Na_{10}[(UO_2)(SO_4)_4](SO_4)_2(H_2O)_3$
Crystal system, space group	Monoclinic, *Cc*
Temperature (K)	293(2)
a, *b*, *c* (Å)	9.3134(4), 28.7501(11), 9.6346(7)
β (°)	93.442(7)
V (Å^3)	2575.1(2)
Z	4
Density (for above formula) (g cm^{-3})	2.916
Absorption coefficient (mm^{-1})	7.083
Data collection	
Diffractometer	Rigaku R-Axis Rapid II
X-ray radiation/power	Mo*K*α (λ = 0.71075 Å)/50 kV, 40 mA
F(000)	2144
Crystal size (μm)	290 × 80 × 50
θ range (°)	3.05 to 27.48
No. of measured, independent and observed [$I > 2\sigma I$] reflections	11365, 5423, 5202
R_{int}	0.044
Index ranges	$-11 \le h \le 12$, $-36 \le k \le 36$, $-12 \le l \le 11$
Completeness to θ = 27.48°	98.3%
Refinement	
Refinement method	Full-matrix least-squares on F^2
No. parameters/restraints	416/2
GoF	1.077
Final *R* indices [$I > 2\sigma I$]	$R_1 = 0.0298$, $wR_2 = 0.0674$
R indices (all data)	$R_1 = 0.0320$, $wR_2 = 0.0694$
Absolute structure parameter	0.302(6)
Largest diff. peak/hole (e^- A^{-3})	+2.28/–0.64

$R_{int} = \Sigma|F_o^2 - F_o^2(\text{mean})|/\Sigma[F_o^2]$. GoF = $S = \{\Sigma[w(F_o^2 - F_c^2)^2]/(n-p)\}^{1/2}$. $R_1 = \Sigma||F_o| - |F_c||/\Sigma|F_o|$. $wR_2 = \{\Sigma[w(F_o^2 - F_c^2)^2]/\Sigma[w(F_o^2)^2]\}^{1/2}$; $w = 1/[\sigma^2(F_o^2) + (aP)^2 + bP]$ where *a* is 0.0225, *b* is 0 and *P* is $[2F_c^2 + \text{Max}(F_o^2, 0)]/3$.

Table 4. Atom coordinates and equivalent isotropic displacement parameters (Å^2) for lussierite.

	x/*a*	*y*/*b*	*z*/*c*	U_{eq}
U	0.65915(5)	0.82751(2)	0.16668(5)	0.01384(9)
S1	0.8933(3)	0.84073(11)	0.4052(3)	0.0146(5)
S2	0.3898(3)	0.83781(11)	0.8969(3)	0.0156(6)
S3	0.8123(3)	0.83512(8)	0.8192(2)	0.0149(5)
S4	0.5583(3)	0.96841(7)	0.5704(2)	0.0170(4)
S5	0.9928(3)	0.96595(8)	0.9928(2)	0.0167(4)
S6	0.8072(3)	0.66357(8)	0.8161(2)	0.0151(5)
Na1	0.6512(12)	0.32356(12)	0.6568(11)	0.0229(10)
Na2	0.7943(6)	0.74727(18)	0.5754(5)	0.0338(12)
Na3	0.5386(5)	0.74998(18)	0.7852(5)	0.0309(11)
Na4	0.5531(5)	0.86097(17)	0.5815(5)	0.0320(11)
Na5	0.6584(5)	0.93550(16)	0.9100(4)	0.0282(10)
Na6	0.7800(5)	0.95919(15)	0.2874(4)	0.0295(9)
Na7	0.6997(5)	0.56780(16)	0.9538(4)	0.0355(10)
Na8	0.8919(5)	0.93482(15)	0.6456(4)	0.0301(9)
Na9	0.8471(5)	0.56283(14)	0.5975(4)	0.0304(9)
Na10	0.5614(5)	0.63823(17)	0.5710(5)	0.0321(10)
O1	0.6866(9)	0.2332(2)	0.6807(10)	0.027(2)
O2	0.6352(10)	0.8889(2)	0.1568(10)	0.027(2)
O3	0.9563(10)	0.6791(3)	0.7857(10)	0.042(2)
O4	0.7933(11)	0.8340(3)	0.9713(8)	0.040(2)
O5	0.4898(8)	0.8070(2)	0.9896(7)	0.0271(16)
O6	0.4082(8)	0.6630(2)	0.7519(6)	0.0220(15)
O7	0.7344(8)	0.8380(2)	0.4170(7)	0.0227(15)
O8	0.9517(9)	0.8848(3)	0.4544(8)	0.0320(19)
O9	0.9618(7)	0.8015(2)	0.4765(7)	0.0237(15)
O10	0.7443(9)	0.6724(2)	0.4356(9)	0.0313(18)
O11	0.4280(8)	0.8866(3)	0.9186(7)	0.0258(18)
O12	0.4081(9)	0.8230(2)	0.7531(7)	0.0254(16)
O13	0.9636(12)	0.8331(4)	0.8037(12)	0.063(3)
O14	0.7370(10)	0.7969(3)	0.7518(8)	0.044(2)
O15	0.7551(14)	0.8785(3)	0.7633(10)	0.053(3)
O16	0.6702(9)	0.9469(3)	0.4916(8)	0.0363(19)
O17	0.6198(9)	0.9814(3)	0.7077(7)	0.039(2)
O18	0.4417(9)	0.9345(2)	0.5849(8)	0.0345(18)
O19	0.0000(9)	0.4894(2)	0.9995(7)	0.0275(16)
O20	0.3983(10)	0.5566(3)	0.5896(8)	0.044(2)
O21	0.9115(10)	0.9728(3)	0.8598(8)	0.044(2)
O22	0.5448(9)	0.4893(2)	0.5477(8)	0.0301(18)
O23	0.6177(8)	0.4347(3)	0.9743(7)	0.0289(16)
O24	0.7088(8)	0.6959(3)	0.7469(7)	0.0302(17)
O25	0.7985(12)	0.6638(3)	0.9656(9)	0.046(2)
O26	0.7837(11)	0.6174(3)	0.7591(10)	0.041(2)
O27 (H_2O)	0.6849(8)	0.4074(2)	0.7034(7)	0.0261(16)
O28 (H_2O)	0.5253(11)	0.7494(3)	0.5195(9)	0.043(2)
O29 (H_2O)	0.7765(10)	0.5142(3)	0.7812(8)	0.0323(18)

were only partially successful. Analyses exhibited large variations in Na content, always yielding values significantly below those indicated by the structure refinement, which was consistent with stoichiometric Na (see below). Consequently, we have used the calculated Na content corresponding to 10 Na atoms per formula unit (apfu). U and S exhibited time-dependent ingrowth during analysis for which a correction was applied. No other elements (including N) were detected by energy- or wavelength-dispersive spectroscopy. Due to the limited amount of material available, the H_2O content could not be measured and is instead calculated by stoichiometry based on 6 S and 29 O apfu as indicated by the structure. The loss of loosely bound H_2O under vacuum apparently results in higher concentrations for the remaining constituents than are to be expected for the fully hydrated phase and is probably the cause of the high analytical total. Analytical data are given in Table 1. The empirical formula (calculated on the basis of 29 O apfu) is $Na_{10}(U_{0.99}O_2)(S_{1.00}O_4)_6{\cdot}3H_2O$ (+0.06 H for charge balance). The ideal formula is $Na_{10}[(UO_2)(SO_4)_4](SO_4)_2(H_2O)_3$, which requires Na_2O 27.42, UO_3 25.31, SO_3 42.50, H_2O 4.78, total 100 wt.%.

X-ray crystallography and structure refinement

Powder X-ray studies were carried out using a Rigaku R-Axis Rapid II curved imaging plate microdiffractometer, with monochromatic Mo*K*α radiation. A Gandolfi-like motion on the φ and ω axes was used to randomise the samples and observed *d* values and intensities were derived by profile fitting using *JADE 2010* software (Materials Data, Inc.). The observed powder data for lussierite, presented in Table 2, show good agreement with the pattern calculated from the structure refinement. The unit-cell parameters refined from the powder data using *JADE 2010* with whole pattern fitting are *a* = 9.3134(4), *b* = 28.7501(11), *c* = 9.6346(7) Å, β = 93.442(7)° and *V* = 2575.1(2) Å^3.

Single-crystal X-ray studies were done using the same diffractometer and radiation used for the powder studies. The Rigaku *CrystalClear* software package was used for processing the structure data, including the application of an empirical absorption correction using the multi-scan method with *ABSCOR* (Higashi, 2001). The structure was solved in space group *Cc* using *SIR2011* (Burla *et al.*, 2012). *SHELXL-2016* (Sheldrick, 2015) was used for the refinement of the structure. The structure was noted to be the same as that determined for synthetic $Na_{10}[(UO_2)(SO_4)_4](SO_4)_2{\cdot}3H_2O$ by Burns and Hayden (2002). Consequently, equivalent atoms were assigned the same numbers in the lussierite structure. Both structures exhibit merohedral twinning, but have different dominant twin components. All non-

Table 5. Anisotropic displacement parameters for lussierite.

	U^{11}	U^{22}	U^{33}	U^{23}	U^{13}	U^{12}
U	0.01461(16)	0.01500(14)	0.01176(14)	0.00140(16)	−0.00053(9)	−0.00018(18)
S1	0.0154(13)	0.0177(12)	0.0107(12)	0.0006(10)	0.0001(9)	0.0017(10)
S2	0.0163(14)	0.0171(12)	0.0130(12)	−0.0012(9)	−0.0023(9)	−0.0002(10)
S3	0.0161(12)	0.0174(11)	0.0113(11)	−0.0012(8)	0.0030(8)	−0.0010(9)
S4	0.0229(13)	0.0136(10)	0.0146(10)	0.0009(8)	0.0021(8)	0.0005(9)
S5	0.0210(12)	0.0141(11)	0.0153(10)	−0.0004(8)	0.0037(8)	0.0006(9)
S6	0.0157(13)	0.0174(11)	0.0122(11)	−0.0011(8)	0.0019(8)	0.0017(9)
Na1	0.018(2)	0.0294(18)	0.022(3)	−0.002(2)	0.0005(18)	−0.004(2)
Na2	0.043(3)	0.025(3)	0.036(3)	−0.0009(19)	0.022(2)	−0.004(2)
Na3	0.032(3)	0.020(3)	0.042(2)	0.0042(19)	0.0169(19)	0.003(2)
Na4	0.033(3)	0.033(3)	0.031(2)	−0.001(2)	0.0054(18)	0.003(2)
Na5	0.034(3)	0.027(2)	0.025(2)	0.0010(16)	0.0064(17)	0.0041(17)
Na6	0.043(3)	0.023(2)	0.023(2)	0.0008(16)	0.0084(16)	−0.0001(19)
Na7	0.046(3)	0.032(3)	0.030(2)	0.0014(19)	0.0132(19)	−0.009(2)
Na8	0.045(3)	0.026(2)	0.019(2)	−0.0034(15)	0.0077(16)	−0.0049(18)
Na9	0.040(3)	0.026(2)	0.026(2)	0.0013(16)	0.0086(16)	0.0089(19)
Na10	0.029(3)	0.039(3)	0.029(2)	−0.009(2)	0.0064(17)	−0.002(2)
O1	0.025(6)	0.020(3)	0.036(5)	−0.007(3)	0.000(4)	−0.003(3)
O2	0.036(6)	0.018(3)	0.027(4)	0.001(3)	−0.004(4)	0.000(3)
O3	0.023(5)	0.055(6)	0.047(5)	−0.020(4)	0.010(4)	−0.003(4)
O4	0.050(6)	0.055(6)	0.013(4)	0.007(3)	0.001(4)	−0.011(4)
O5	0.035(4)	0.015(3)	0.030(4)	0.000(3)	−0.011(3)	0.005(3)
O6	0.021(4)	0.034(4)	0.011(3)	0.004(3)	0.004(3)	0.002(3)
O7	0.022(4)	0.027(4)	0.019(3)	−0.005(3)	0.004(3)	−0.002(3)
O8	0.041(6)	0.021(4)	0.034(4)	−0.011(3)	0.000(4)	−0.011(4)
O9	0.021(4)	0.023(4)	0.027(4)	0.010(3)	0.002(3)	0.001(3)
O10	0.016(4)	0.042(5)	0.036(4)	−0.005(3)	0.003(3)	0.003(3)
O11	0.035(5)	0.015(4)	0.026(4)	0.003(3)	−0.006(3)	0.000(3)
O12	0.034(5)	0.028(4)	0.014(3)	−0.005(3)	0.003(3)	0.003(3)
O13	0.024(6)	0.126(11)	0.042(6)	−0.009(5)	0.012(4)	0.001(5)
O14	0.063(6)	0.036(5)	0.033(4)	−0.016(4)	0.015(4)	−0.029(4)
O15	0.095(9)	0.027(5)	0.036(5)	0.011(4)	0.001(5)	0.008(5)
O16	0.043(5)	0.033(5)	0.034(4)	0.002(3)	0.013(3)	0.015(4)
O17	0.061(6)	0.032(4)	0.022(4)	−0.004(3)	−0.011(3)	−0.009(4)
O18	0.038(5)	0.022(4)	0.043(5)	0.008(3)	0.000(3)	−0.010(3)
O19	0.038(5)	0.020(4)	0.025(4)	−0.004(3)	0.004(3)	−0.006(3)
O20	0.064(6)	0.033(5)	0.039(5)	0.008(4)	0.029(4)	0.017(4)
O21	0.060(6)	0.048(5)	0.021(4)	−0.009(3)	−0.014(4)	0.024(4)
O22	0.042(5)	0.013(4)	0.037(4)	0.006(3)	0.014(3)	0.003(4)
O23	0.032(4)	0.026(4)	0.028(4)	−0.007(3)	−0.002(3)	0.011(3)
O24	0.029(4)	0.031(4)	0.031(4)	0.010(3)	0.007(3)	0.014(3)
O25	0.056(7)	0.065(6)	0.019(5)	−0.002(4)	0.009(4)	0.026(5)
O26	0.059(7)	0.017(4)	0.049(5)	−0.009(4)	0.012(4)	−0.002(4)
O27	0.033(5)	0.021(3)	0.024(4)	0.003(3)	0.000(3)	0.004(3)
O28	0.058(6)	0.034(5)	0.035(4)	0.005(3)	−0.020(4)	−0.004(4)
O29	0.041(5)	0.022(4)	0.035(4)	−0.001(4)	0.008(3)	−0.002(4)

hydrogen atoms were successfully refined with full occupancies and anisotropic displacement parameters. Because the electron microprobe analysis provided much lower than stoichiometric Na, an attempt was made to refine the occupancies of the Na sites; however, all refined to very close to full occupancy and did not improve the *R* factor. Difference-Fourier maps failed to reveal possible H sites. Data collection and refinement details are given in Table 3, atom coordinates and equivalent isotropic displacement parameters in Table 4, anisotropic displacement parameters in Table 5, selected bond distances in Table 6 and a bond-valence analysis in Table 7. The crystallographic information files have been deposited with the Principal Editor of *Mineralogical Magazine* and are available as Supplementary material (see below).

During the course of checking numerous lussierite crystals, one crystal examined provided the cell: $a = 9.3141(7)$, $b = 86.264(5)$, $c = 9.6317(7)$ Å and $\beta = 93.391(7)°$. The structure of this crystal, also solved in space group *Cc*, indicates it to be the 3*M* polytype: lussierite-3*M*. The structure refinement was significantly poorer than that noted above (only the U atoms could be refined anisotropically). Notably, the powder X-ray diffraction pattern calculated from this structure fits the observed lussierite powder X-ray diffraction pattern equally well.

Description of the structure

The U site in the structure of lussierite is surrounded by seven O atom sites forming a squat pentagonal bipyramid. This is a typical coordination for U^{6+} in which the two short apical bonds of the bipyramid constitute the uranyl group (*cf.* Burns, 2005). The two apical O atoms of the bipyramid (O_{Ur}) form short bonds with the U, and this unit comprises the UO_2^{2+} uranyl group. The five equatorial O atoms (O_{eq}) complete the U coordination and link to four different SO_4 tetrahedra in the structure. Three of these SO_4 tetrahedra (S1, S2 and S3) share single equatorial O atoms, while one (S6) shares two of its O atoms

Table 6. Selected bond distances (Å) for lussierite.

U–O1	1.769(7)	Na1–O13	2.330(15)	Na6–O16	2.298(9)
U–O2	1.782(6)	Na1–O25	2.390(14)	Na6–O20	2.303(8)
U–O3	2.276(9)	Na1–O27	2.470(8)	Na6–O17	2.366(9)
U–O4	2.328(9)	Na1–O9	2.483(12)	Na6–O21	2.389(9)
U–O5	2.328(7)	Na1–O12	2.514(13)	Na6–O2	2.698(8)
U–O6	2.429(7)	Na1–O1	2.626(8)	<Na6–O>	2.411
U–O7	2.489(7)	Na1–O10	2.775(12)		
<U–O$_{Ur}$>	1.776	<Na1–O>	2.513	Na7–O22	2.398(9)
<U–O$_{eq}$>	2.370			Na7–O29	2.406(9)
		Na2–O14	2.306(9)	Na7–O26	2.518(10)
S1–O8	1.447(8)	Na2–O24	2.389(9)	Na7–O18	2.518(9)
S1–O9	1.449(7)	Na2–O9	2.438(8)	Na7–O27	2.519(8)
S1–O7	1.494(8)	Na2–O28	2.532(11)	Na7–O8	2.682(9)
S1–O6	1.496(7)	Na2–O10	2.567(9)	Na7–O25	2.911(11)
<S1–O>	1.472	Na2–O5	2.573(9)	<Na7–O>	2.565
		<Na2–O>	2.468		
S2–O10	1.456(9)			Na8–O21	2.332(8)
S2–O11	1.460(8)	Na3–O24	2.267(9)	Na8–O22	2.353(9)
S2–O12	1.470(7)	Na3–O14	2.326(10)	Na8–O15	2.389(12)
S2–O5	1.532(7)	Na3–O12	2.436(9)	Na8–O8	2.428(8)
<S2–O>	1.480	Na3–O9	2.501(9)	Na8–O16	2.493(9)
		Na3–O28	2.555(10)	Na8–O27	2.863(9)
S3–O13	1.427(11)	Na3–O5	2.623(9)	Na8–O17	2.958(10)
S3–O14	1.437(8)	Na3–O6	2.791(9)	<Na8–O>	2.545
S3–O15	1.446(9)	<Na3–O>	2.500		
S3–O4	1.487(8)			Na9–O19	2.309(8)
<S3–O>	1.449	Na4–O18	2.356(9)	Na9–O26	2.312(9)
		Na4–O12	2.452(9)	Na9–O29	2.378(9)
S4–O17	1.458(7)	Na4–O7	2.473(9)	Na9–O23	2.382(8)
S4–O16	1.463(8)	Na4–O15	2.543(11)	Na9–O11	2.409(8)
S4–O18	1.472(8)	Na4–O25	2.657(11)	<Na9–O>	2.358
S4–O19	1.480(7)	Na4–O16	2.855(10)		
<S4–O>	1.468	Na4–O14	2.947(11)	Na10–O23	2.367(9)
		<Na4–O>	2.612	Na10–O10	2.416(10)
S5–O22	1.462(7)			Na10–O6	2.425(8)
S5–O21	1.463(7)	Na5–O19	2.339(9)	Na10–O24	2.688(9)
S5–O20	1.470(8)	Na5–O17	2.363(8)	Na10–O26	2.736(11)
S5–O23	1.489(7)	Na5–O15	2.377(12)	Na10–O4	2.740(11)
<S5–O>	1.471	Na5–O11	2.571(9)	Na10–O13	2.803(12)
		Na5–O21	2.660(12)	Na10–O20	2.808(10)
S6–O24	1.439(7)	Na5–O2	2.748(10)	<Na10–O>	2.623
S6–O25	1.448(9)	Na5–O20	2.752(10)		
S6–O26	1.448(8)	<Na5–O>	2.544		
S6–O3	1.505(9)				
<S6–O>	1.460				

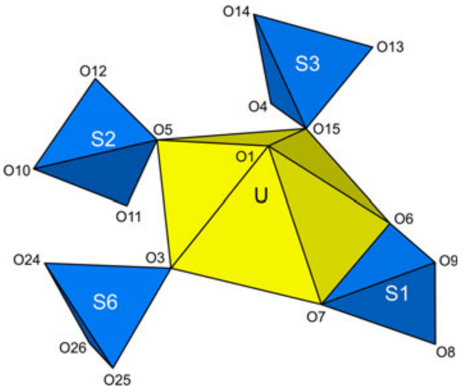

Fig. 5. The $[(UO_2)(SO_4)_4]^{6-}$ uranyl sulfate cluster in the structure of lussierite.

with the U1 bipyramid, thereby linking along a polyhedral edge. Such a bidentate linkage between a UO_7 pentagonal bipyramid and a SO_4 tetrahedron has been previously reported in the Na uranyl sulfate minerals klaprothite, péligotite and ottohahnite, which also occur at the Blue Lizard mine (Kampf *et al.*, 2017). The $[(UO_2)(SO_4)_4]^{6-}$ uranyl sulfate cluster (Fig. 5) is the fundamental building block (*FBB*) in the structure of lussierite. It is also the *FBB* in the structures of klaprothite and péligotite; while in the structure of ottohahnite, four of these uranyl sulfate clusters are combined through shared SO_4 tetrahedra to form a larger $[(UO_2)_4(SO_4)_{10}]^{12-}$ cluster.

The uranyl sulfate clusters occur in layers parallel to {010} and are linked through a complex network of bonds involving 10 different Na^+ cations, two isolated SO_4 tetrahedra (S4 and S5) and three H_2O groups (Fig. 6). Na–O coordination varies from 5 to 8. Isolated SO_4 tetrahedra are rare in the structures of uranyl sulfates; however, they have been observed, for example, in

Table 7. Bond-valence analysis for lussierite. Values are expressed in valence units.*

	U	S1	S2	S3	S4	S5	S6	Na1	Na2	Na3	Na4	Na5	Na6	Na7	Na8	Na9	Na10	Sum
O1	1.80							0.11										1.91
O2	1.75											0.08	0.09					1.92
O3	0.61						1.38											2.00
O4	0.55			1.45													0.08	2.08
O5	0.55		1.29						0.12	0.11								2.08
O6	0.44	1.41								0.07							0.18	2.11
O7	0.39	1.42									0.16							1.97
O8		1.60												0.10	0.17			1.87
O9		1.59						0.15	0.17	0.15								2.06
O10			1.56					0.08	0.13								0.18	1.94
O11			1.55									0.12				0.18		1.85
O12			1.51					0.14		0.17	0.16							1.99
O13				1.68				0.22									0.07	1.97
O14				1.64					0.23	0.22	0.05							2.15
O15				1.60							0.13	0.20			0.19			2.12
O16					1.54						0.06		0.24		0.15			1.99
O17					1.55							0.20	0.20		0.05			2.01
O18					1.50						0.21			0.14				1.85
O19					1.47							0.22				0.23		1.92
O20						1.51						0.08	0.24				0.07	1.89
O21						1.54						0.10	0.19		0.22			2.05
O22						1.54								0.19	0.21			1.94
O23						1.44										0.19	0.20	1.83
O24							1.63		0.19	0.26							0.09	2.17
O25							1.59	0.19			0.10			0.06				1.94
O26							1.59							0.14		0.23	0.08	2.05
O27								0.16						0.14	0.06			0.36
O28									0.14	0.13								0.27
O29														0.18		0.20		0.38
Sum	6.10	6.02	5.91	6.37	6.06	6.02	6.20	1.05	0.98	1.11	0.88	1.00	0.96	0.94	1.06	1.04	0.96	

*All bond valence parameters are from Gagné and Hawthorne (2015). Hydrogen bonds are not included. Note that O27, O28 and O29 are O atoms of H_2O groups.

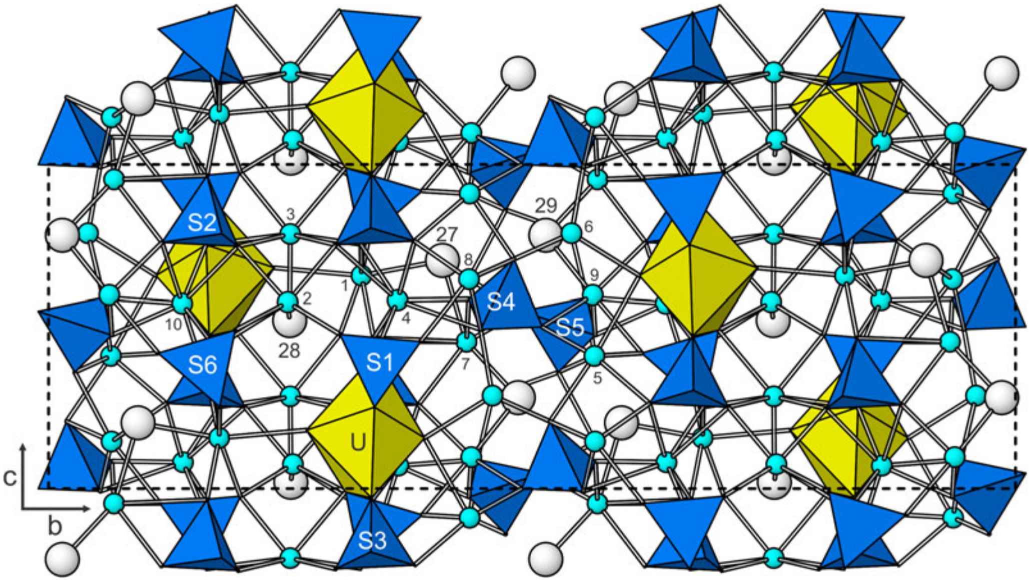

Fig. 6. The crystal structure of lussierite. The unit cell is indicated by dashed lines. The Na atoms are shown as small turquoise spheres (labelled with small numbers). The O atoms of H_2O groups are shown as white spheres (labelled with large numbers). Na–O bonds are drawn as sticks.

belakovskiite, which contains $[(UO_2)(SO_4)_4(H_2O)]^{6-}$ *FBB*s (with monodentate U–S linkage) (Kampf *et al.*, 2014).

Acknowledgements. Reviewer Igor V. Pekov, Structures Editor Peter Leverett and an anonymous reviewer are thanked for their constructive comments on the manuscript. A portion of this study was funded by the John Jago Trelawney Endowment to the Mineral Sciences Department of the Natural History Museum of Los Angeles County. This research was also financially supported by the Czech Science Foundation (project GACR 17–09161S to JP).

Supplementary material. To view supplementary material for this article, please visit https://doi.org/10.1180/mgm.2019.34.

References

Bartlett J.R. and Cooney R.P. (1989) On the determination of uranium-oxygen bond lengths in dioxouranium(VI) compounds by Raman spectroscopy. *Journal of Molecular Structure*, **193**, 295–300.

Bosi F., Andreozzi G.B., Skogby H., Lussier A.J., Abdu Y.A. and Hawthorne F.C. (2013) Fluor-elbaite, $Na(Li_{1.5}Al_{1.5})Al_6(Si_6O_{18})(BO_3)_3(OH)_3F$, a new mineral species of the tourmaline supergroup. *American Mineralogist*, **98**, 297–303.

Burla M.C., Caliandro R., Camalli M., Carrozzini B., Cascarano G.L., Giacovazzo C., Mallamo M., Mazzone A., Polidori G. and Spagna R. (2012) *SIR*2011: a new package for crystal structure determination and refinement. *Journal of Applied Crystallography*, **45**, 357–361.

Burns P.C. (2005) U^{6+} minerals and inorganic compounds: insights into an expanded structural hierarchy of crystal structures. *The Canadian Mineralogist*, **43**, 1839–1894.

Burns P.C. and Hayden L.A. (2002) A uranyl sulfate cluster in $Na_{10}[(UO_2)(SO_4)_4](SO_4)_2{\cdot}3H_2O$. *Acta Crystallographica*, **C58**, i121–i123.

Čejka J. (1999) Infrared spectroscopy and thermal analysis of the uranyl minerals. Pp. 521–622. *Uranium: Mineralogy, Geochemistry and the Environment* (P.C. Burns and R.C. Finch, editors). Reviews in Mineralogy, **38**. Mineralogical Society of America, Washington, DC.

Chenoweth W.L. (1993) The geology and production history of the uranium deposits in the White Canyon Mining District, San Juan County, Utah. *Utah Geological Survey Miscellaneous Publication*, **93–3**.

Gagné O.C. and Hawthorne F.C. (2015) Comprehensive derivation of bond-valence parameters for ion pairs involving oxygen. *Acta Crystallographica*, **B71**, 562–578.

Gurzhiy V.V. and Plášil J. (2019) Structural complexity of natural uranyl sulfates. *Acta Crystallographica*, **B75**, 39–48.

Hawthorne F.C., Lussier A.J., Ball N.A., Henry D.J., Shimizu R., Ogasawara Y. and Ota T. (2016) Maruyamaite, $K(MgAl_2)(Al_5Mg)Si_6O_{18}(BO_3)_3(OH)_3O$, from the ultrahigh–pressure Kokchetav massif, northern Kazakhstan: Description and crystal structure. *American Mineralogist*, **101**, 355–361.

Higashi T. (2001) *ABSCOR*. Rigaku Corporation, Tokyo.

Kampf A.R., Plášil J., Kasatkin A.V. and Marty J. (2014) Belakovskiite, $Na_7(UO_2)(SO_4)_4(SO_3OH)(H_2O)_3$, a new uranyl sulfate mineral from the Blue Lizard mine, San Juan County, Utah, USA. *Mineralogical Magazine*, **78**, 639–649.

Kampf A.R., Plášil J., Kasatkin A.V. and Marty J. (2015) Bobcookite, $NaAl(UO_2)_2(SO_4)_4{\cdot}18H_2O$, and wetherillite, $Na_2Mg(UO_2)_2(SO_4)_4{\cdot}18H_2O$, two new uranyl sulfate minerals from the Blue Lizard mine, San Juan County, Utah, USA. *Mineralogical Magazine*, **79**, 695–714.

Kampf A.R., Plášil J., Kasatkin A.V., Marty J. and Čejka J. (2017) Klaprothite, péligotite and ottohahnite, three new minerals with bidentate UO_7–SO_4 linkages from the Blue Lizard mine, San Juan County, Utah, USA. *Mineralogical Magazine*, **81**, 753–779.

Kampf A.R., Olds T., Plášil J., Nash B.P. and Marty J. (2018) Lussierite, IMA 2018-101. CNMNC Newsletter No. 46, December 2018, page 1376; *Mineralogical Magazine*, **82**, 1369–1379.

Libowitzky E. (1999) Correlation of O–H stretching frequencies and O–H···O hydrogen bond lengths in minerals. *Monatshefte für Chemie*, **130**, 1047–1059.

Lussier A.J. (2012) *Zonation in Tourmaline from Granitic Pegmatites and the Occurrence of Tetrahedrally Coordinated Aluminum and Boron in Tourmaline*. PhD thesis, Manitoba, Canada.

Lussier A.J., Hawthorne F.C., Abdu Y.A., Ball N.A., Tait K.T., Back M.E., Steede A.H., Taylor R. and McDonald A.M. (2014) Ferro-ferri-nybøite, $NaNa_2(Fe^{2+}_3Fe^{3+}_2)Si_8O_{22}(OH)_2$, a new clinoamphibole from Mont Saint-Hilaire, Québec, Canada: Description and crystal structure. *The Canadian Mineralogist*, **52**, 1019–1026.

Lussier A.J., Lopez R.A.K. and Hawthorne F.C. (2016) A revised and expanded structure hierarchy of natural and synthetic hexavalent uranium compounds. *The Canadian Mineralogist*, **54**, 177–283.

Mandarino J.A. (1976) The Gladstone–Dale relationship – Part 1: derivation of new constants. *The Canadian Mineralogist*, **14**, 498–502.

Olds T.A., Lussier A.J., Oliver A. G., Petrˇíček V., Plášil J., Kampf A.R., Burns P.C., Dembowski M., Carlson S.M. and Steele I.M. (2017) Shinkolobweite, IMA 2016-095. CNMNC Newsletter No. 36, April 2017, page 404; *Mineralogical Magazine*, **81**, 403–409.

Plášil J., Buixaderas E., Čejka J., Sejkora J., Jelička J., and Novk M. (2010) Raman spectroscopic study of the uranyl sulphate mineral zippeite: low wavenumber and U–O stretching regions. *Analytical and Bioanalytical Chemistry*, **397**, 2703–2715.

Plášil J., Kampf A.R., Kasatkin A.V. and Marty J. (2014) Bluelizardite, $Na_7(UO_2)(SO_4)_4Cl(H_2O)_2$, a new uranyl sulfate mineral from the Blue Lizard mine, San Juan County, Utah, USA. *Journal of Geosciences*, **59**, 145–158.

Pouchou J.L. and Pichoir F. (1985) "PAP" (φρZ) procedure for improved quantitative microanalysis. Pp. 104–106 in: *Microbeam Analysis* (J.T. Armstrong, editor). San Francisco Press, San Francisco, California, USA.

Sheldrick G.M. (2015) Crystal structure refinement with *SHELX*. *Acta Crystallographica*, **C71**, 3–8.

Volkovich V.A., Griffiths T.R., Fray D.J. and Fields M. (1998) Vibrational spectra of alkali metal Li, Na and K uranates and consequent assignment of uranate ion site symmetry. *Vibrational Spectroscopy*, **17**, 83–91.